Journal of Catalysis 270 (2010) 214–223

Contents lists available at ScienceDirect

Journal of Catalysis

journal homepage: www.elsevier.com/locate/jcat

Isotopic studies of NO_X storage and reduction on $Pt/BaO/Al_2O_3$ catalyst using temporal analysis of products

Ashok Kumar, Michael P. Harold *, Vemuri Balakotaiah *

Department of Chemical and Biomolecular Engineering, University of Houston, Houston, TX 77204-4004, United States

ARTICLE INFO

Article history:
Received 14 September 2009
Revised 2 December 2009
Accepted 25 December 2009
Available online 2 February 2010

Keywords:
NO_X
Lean NO_X trap
Platinum
Temporal analysis of products (TAP)
Spillover

ABSTRACT

A systematic isotopic study over $Pt/BaO/Al_2O_3$ powder catalyst was carried out using temporal analysis of products (TAP) to elucidate the role of the Pt/BaO interface and spillover processes during NO_X storage and reduction. The sequential pre-nitration of $Pt/BaO/Al_2O_3$ using NO and ^{15}NO followed by reduction with H_2 results in the preferential evolution of ^{15}N-containing species during initial H_2 pulses. The evolution shifts toward unlabeled N-containing species in later H_2 pulses. The data suggest that NO_X storage proceeds radially outward from the Pt crystallites and that some mobility of the stored NO_X species exists. The evolution of N_2 and ^{15}NN during $^{15}NO–H_2$ pump–probe on a pre-nitrated (using unlabeled NO) catalyst confirms the involvement of spillover processes at the Pt/BaO interface. The evolution of nitrogen takes place by NO decomposition as well as by the reaction of stored NO_X with H_2 to form adsorbed N and eventually N_2. A significant fraction of N_2 is also produced via NH_3 serving as an intermediate. The results suggest that the local gradients at the Pt/BaO interface in the stored NO_X are important and that these should be taken into account in NSR catalyst design and modeling.

1. Introduction

Engines that operate under lean conditions have significantly better fuel economy compared to stoichiometric engines. However, in the presence of excess oxygen in the exhaust, NO_X cannot be effectively reduced by conventional three-way catalysts. An emerging technology for NO_X removal from lean burn engines is NO_X storage and reduction (NSR). NSR involves storage of NO_X on an alkaline earth component (Ba, Ca) mediated by precious metals (Pt, Rh) and followed by the intermittent injection of a rich pulse for a shorter duration to reduce the stored NO_X to desired product N_2.

The chemistry and kinetics of the NSR are of keen interest to the catalysis community due to both its technological importance in air pollution control and its complexity manifested by the transient operation, multifunctional catalyst and coupling between reaction and transport processes [1–4]. Comprehensive reviews have appeared in Epling et al. [5], Guthenke et al. [6] and Roy and Baiker [7]. The precious metal function (Pt) catalyzes NO oxidation to NO_2 and stored NO_X reduction. The storage function (BaO) traps NO_X in the form of nitrites and/or nitrates directly through the gas phase and/or by NO_X spillover from Pt. Many atmospheric flow reactor experiments, modeling and surface science studies have been performed to better understand and unravel the chemistry, kinetics and performance features of the lean NO_X trap (LNT). The importance of coupling between the precious metal and storage function (BaO) is by now recognized, building on the early results of Mahzoul et al. [8].

Temporal analysis of products (TAP), developed by Gleaves and coworkers [9–11], has proven its utility in a host of catalytic reaction systems ([11,12] and references within). It is well suited for NSR, an inherently transient catalytic process. Kabin et al. [1] used TAP to study NO and NO_2 adsorption and decomposition on $Pt/BaO/Al_2O_3$. Medhekar et al. [13] studied NSR chemistry and Pt/BaO coupling on pre-reduced, pre-oxidized and pre-nitrated $Pt/BaO/Al_2O_3$ with NO pulsing and $NO–H_2$ pump–probe experiments. More recently, Kumar et al. [14] studied the effect of the delay time between consecutive NO and H_2 pulses on the selectivities of N_2 and NH_3 using both powder and monolith Pt/Al_2O_3 catalysts.

NSR renders itself to isotopic experiments in order to identify reaction pathways, mechanisms and kinetics. Breen et al. [15] used isotopic labeling (^{15}NO) coupled with fast transient kinetic switching during NSR. They used ^{15}NO instead of NO to differentiate $^{15}N_2$ from CO and $^{15}N_2O$ from CO_2 in the mass spectrometric analysis. The use of labeled species allowed a more detailed analysis of the products and reactants involved in the regeneration of a NSR material. Cant et al. [16] compared the isotopic exchange rate of ^{15}NO and stored unlabeled NO_X during storage on $Pt/BaO/Al_2O_3$ and a physical mixture of Pt/SiO_2 and BaO/Al_2O_3 at 360 °C. They concluded that the forward and reverse spillover of NO_X is

* Corresponding authors.
E-mail addresses: mharold@uh.edu (M.P. Harold), bala@uh.edu (V. Balakotaiah).

0021-9517/$ - see front matter © 2009 Elsevier Inc. All rights reserved.
doi:10.1016/j.jcat.2009.12.018

important, since the exchange rate was more than five times faster for $Pt/BaO/Al_2O_3$ sample than the physical mixture.

The storage of NO in the presence of excess oxygen proceeds through both nitrate and nitrite routes. NO is oxidized on Pt sites and directly stored on neighboring BaO sites in the form of nitrites that are then oxidized to nitrates [17]. Mahzoul et al. [8] proposed that two kinds of Pt sites, one close to barium and the other far from barium, are responsible for nitrate formation and NO oxidation, respectively. Lindholm et al. [18], in their model of NO_X storage and reduction in the presence of H_2O and CO_2, proposed two kinds of barium sites, one close and others far from the noble metal. Recently, Bhatia et al. [19] also described two kinds of barium sites, namely fast and slow sites, which are, respectively, near and far from Pt/BaO interface, in order to explain NO_X storage and reduction during atmospheric condition experiments. Sakamoto et al. [20] studied NO_X adsorption and desorption phenomena on the Pt/Ba thin film on a Si substrate using electron probe microanalysis (EPMA) for different treatment conditions, temperatures and gas compositions. They observed that NO_X was strongly adsorbed around the edge of the Pt crystallites and that reduction by H_2 occurs preferentially in an area a few micrometers around the Pt. Zhou et al. [21] suggested that nitrate ions are extremely mobile and can migrate to Pt sites where they are reduced in the presence of a reductant. Atmospheric pressure studies over Al_2O_3, Pt/Al_2O_3 and BaO/Al_2O_3 have shown that NO (in the absence of O_2) does not significantly store at 350 °C [22]. NO_X storage and reduction chemistry takes place via reversible spillover processes between Pt and barium sites [23]. Hence, the presence of both precious metal and the storage components is essential for NO_X storage. The reduction of stored nitrates involves a Pt catalyzed surface reaction, and it only occurs when both Pt and BaO are well dispersed on the same support [16,17]. Zhou et al. [21] further emphasize that $Ba(NO_3)_2$ is rather unreactive in the absence of Pt. This was further supported by Clayton et al. [24].

Notwithstanding the progress made by the host of studies during the past 10 years, the distribution and transport of NO_X species during the storage and regeneration on the storage component are still not well understood. In this study, temporal analysis of product (TAP) coupled with isotopic labeling is employed to provide new insight about the mechanism of NO_X storage and reduction on $Pt/BaO/Al_2O_3$. The use of isotopic switching during storage followed by reduction helps to distinguish between uniform and non-uniform distribution of stored NO_X in the barium phase. This study further elucidates the spillover processes and the involvement of Pt/BaO interface during NSR. To this end, the findings are critical to establish a local picture necessary for modeling the performance of NSR catalysts and in designing improved catalysts.

2. Experimental

A Generation-1 TAP reactor system was used following the methodologies described in more detail elsewhere [1,13,14]. The catalyst powder samples of $Pt/BaO/Al_2O_3$ and BaO/Al_2O_3 used for this study were provided by BASF Catalysts LLC (Iselin, NJ). The catalyst powder, $Pt/BaO/Al_2O_3$, having a Pt dispersion of 3.2%, contained 2.48 wt.% Pt and 13.0 wt.% BaO. About 110 mg of $Pt/BaO/Al_2O_3$ catalyst powder was sandwiched between two zones containing inert quartz beads (250–300 μm diameter). The thicknesses of two inert zones were 21 mm and 9 mm while the sandwiched powder zone was 12 mm thick. The estimated number of exposed Pt sites on the catalyst was 2.7×10^{17}. For the independent experiments involving BaO/Al_2O_3 (16.7 wt.% BaO), about 84 mg of powder sample was used to ensure a similar amount of barium as in the first catalyst. In a typical experiment, the catalyst was first reduced by flowing H_2 for 2 h at 400 °C and was then brought down to the reaction temperature (150–350 °C).

The feed contained NO, H_2 and ^{15}NO (98+% isotopic purity, Cambridge Isotope Laboratories). Effluent species including H_2 ($m/e = 2$), N_2 ($m/e = 28$), ^{15}NN ($m/e = 29$), $^{15}N_2$ ($m/e = 30$), NO ($m/e = 30$), ^{15}NO ($m/e = 31$), N_2O ($m/e = 44$), H_2O ($m/e = 18$) and NH_3 ($m/e = 16$) were monitored with a calibrated UTI 100C quadrupole mass spectrometer. The NH_3 signal was measured at $m/e = 16$ because of the overlap with H_2O at $m/e = 17$. Further, $^{15}NH_3$ and H_2O were not measured for the experiments involving $^{15}NH_3$ because of the overlapping signals of H_2O at both $m/e = 18$ and 17. Calibration of NO_2 ($m/e = 46$) was not carried out because it was not detected in the effluent under NO pulsing over $Pt/BaO/Al_2O_3$ or Pt/Al_2O_3 [14]. Moreover, NO_2 does undergoes equilibration under vacuum condition to form NO and O_2 [21], but the absence of O_2 ($m/e = 32$) rules out the formation of gaseous NO_2. Only if NO_2 was fed on an inert bed then it was detected, as reported by Kabin et al. [1].

The gaseous species were calibrated with several hundred pulses on the inert bed reactor. The inlet pulse sizes were calculated by measuring the pressure drop in an isochoric bulb for each gaseous species. The pulse size was correlated with the mass spectrometer signal using a calibration number. The calibration numbers of $^{15}N_2$ and ^{15}NN were assumed to be the same as that of unlabeled N_2, and the calibration number of ^{15}NO was assumed to be same as that of NO. Typically, the mass balances with these calibration numbers have accuracy within 10%. Two principal types of experiments were carried out; these are described next.

2.1. Pulse experiments

These experiments involved the exposure of a large number of consecutive pulses of a single gaseous species (for example NO, ^{15}NO or H_2) to the powder catalyst with a fixed spacing time, τ_s. The typical size of a gaseous pulse was $0.5–2.5 \times 10^{16}$ molecules/pulse, which is about an order of magnitude less than the total number of exposed Pt sites on the $Pt/BaO/Al_2O_3$ catalyst. Unless otherwise stated, the spacing time between successive pulses was 4 s. The pulsing was carried at catalyst bed temperatures ranging between 150 and 350 °C.

2.2. Pump–probe experiments

In a pump–probe experiment, pulses of two different gases were alternatively fed to the catalyst. In this study, we conducted $^{15}NO–H_2$ pump–probe experiments. The duration between successive H_2 and ^{15}NO pulses is the "spacing time" (τ_s), while the duration between the ^{15}NO and H_2 pulse within a single cycle is the "delay time" (τ_d) [14]. In a typical $^{15}NO–H_2$ pump–probe experiment, τ_d was fixed at 4 s, and τ_s was also fixed at 4 s. The ^{15}NO and H_2 pulse intensities were varied by changing the calibrated pulse valve opening times.

3. Results and discussion

3.1. NO storage on $Pt/BaO/Al_2O_3$

NO pulsing experiments were carried out to develop a reproducible method for quantifying the N and O storage on the $Pt/BaO/Al_2O_3$ catalyst. This method was used later in the isotopic studies. NO pulsing on $Pt/BaO/Al_2O_3$ exhibited similar trends previously reported for NO exposure on Pt/Al_2O_3 [13,14] and $Pt/BaO/Al_2O_3$ [13] in the temperature range 150–350 °C (Fig. 1). Note that the solid lines depict the actual profiles while symbols are to distinguish different curves throughout the paper. Average NO pulse

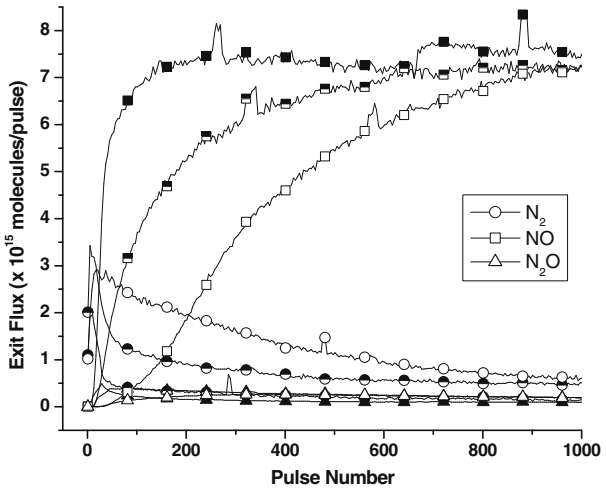

Fig. 1. NO storage on $Pt/BaO/Al_2O_3$ at 150 °C (solid symbols), 250 °C (half filled symbols) and 350 °C (open symbols). The solid lines depict the actual profiles while symbols are to distinguish different curves throughout the paper.

sizes for these experiments were 8.4×10^{15}, 9.8×10^{15} and 9.6×10^{15} molecules/pulse for 150 °C, 250 °C and 350 °C, respectively. As reported previously [13,14], the initial few NO pulses resulted in the formation of N_2, a comparatively much smaller amount of N_2O and essentially no NO. Complete consumption of NO during the initial pulses suggests that NO adsorbs in the front section of the catalyst zone, forming gaseous N_2 and leaving adsorbed oxygen and NO_X on the Pt surface. The adsorbed NO_X then spills over from Pt to BaO and creates vacant Pt sites for further NO adsorption and reaction. This process results in axial gradients of stored NO_X and adsorbed oxygen. As the pulsing of NO continues, the stored NO_X and adsorbed oxygen fronts move downstream in the catalyst zone. When the adsorbed oxygen front reaches the end of the catalyst zone, breakthrough of NO occurs. Here, we define the NO breakthrough point as the point of inflection of the exit NO response. At 150 °C, a sharp breakthrough of NO occurs at about the 30th pulse. A more gradual NO breakthrough occurs at about 45th and 230th pulses for 250 °C and 350 °C, respectively. The earlier NO breakthrough at 150 °C suggests that NO_X storage is smaller for lower temperatures and increases with temperature. The production of N_2, N_2O and consumption of NO at the 1000th pulse show that storage continued to occur well into the experiment.

The stored N, O and the ratio of stored O to stored N on the catalyst were estimated over the course of the multi-pulse experiment using the following balances:

$$N_{Stored}^{Catalyst} = NO_{In} - NO_{Out} - 2N_{2Out} - 2N_2O_{Out} \quad (1)$$

$$O_{Stored}^{Catalyst} = NO_{In} - NO_{Out} - N_2O_{Out} \quad (2)$$

$$\left(\frac{O}{N}\right)_{Stored}^{Catalyst} = \frac{NO_{In} - NO_{Out} - N_2O_{Out}}{NO_{In} - NO_{Out} - 2N_{2Out} - 2N_2O_{Out}} \quad (3)$$

Table 1 reports the calculated N and O stored on the $Pt/BaO/Al_2O_3$ catalyst. The stored N is $(3.9 \pm 0.4) \times 10^{-5}$ and $(3.8 \pm 0.4) \times 10^{-5}$ moles/g catalyst at 250 and 350 °C, respectively. The calculated N storage for the 3.2% Pt dispersed catalyst is about 1.5 times smaller than that of 33% Pt dispersed catalyst previously reported by Medhekar et al. [13] for a similar amount of catalyst and NO exposure. Differences in the N storage for these catalysts are attributed to the ca. 4× smaller number of exposed Pt sites for the 3.2% Pt dispersion catalyst in the current study.

Table 1
Nitrogen and oxygen storage on $Pt/BaO/Al_2O_3$ catalyst and BaO during 1500 NO pulses ($N_{Stored}^{Catalyst}$, $O_{Stored}^{Catalyst}$, O_{Stored}^{BaO} in μmoles/g catalyst).

Temperature (°C)	$N_{Stored}^{Catalyst}$	$O_{Stored}^{Catalyst}$	O_{Stored}^{BaO}	$(O/N)_{Stored}^{Catalyst}$	$(O/N)_{Stored}^{BaO}$
350	38 ± 4	90 ± 5	86 ± 5	2.4 ± 0.1	2.3 ± 0.1
250	39 ± 4	76 ± 5	72 ± 5	1.9 ± 0.1	1.8 ± 0.1

The theoretical ratios of stored O to stored N (i.e. $(O/N)_{Stored}^{BaO}$ for barium nitrate ($Ba(NO_3)_2$) and barium nitrite ($Ba(NO_2)_2$) formation are 2.5 and 1.5, respectively. In the temperature range 250–350 °C, the exposed Pt is preferably occupied by atomic oxygen. Taking atomic oxygen into account, oxygen atoms stored on the barium phase, O_{Stored}^{BaO}, can be estimated. Table 1 shows that the $(O/N)_{Stored}^{BaO}$ over 1500 NO pulses at 350 °C is about 2.3 ± 0.1, which indicates that NO_X is stored mainly in the form of barium nitrate at this temperature. The ratio is about 1.8 ± 0.1 at 250 °C suggesting that NO_X is stored in the form of a mixture of barium nitrates and barium nitrites. At 250 °C, the stored N is essentially the same due to the much larger amount of N_2 produced on the pre-reduced $Pt/BaO/Al_2O_3$ at 350 °C. The N_2 formation results in the accumulation of more oxygen on the catalyst (via NO–Pt + Pt → N–Pt + O–Pt). This feature combined with the recombination of N adatoms to form N_2 (via 2N–Pt → N_2 + 2 Pt) results in a higher $(O/N)_{Stored}^{BaO}$ value at 350 °C, again indicating nitrate formation. Similar storage trends were observed during ^{15}NO pulsing on a pre-reduced catalyst in this temperature range.

There are two plausible pathways for NO_X storage. The first is by the oxidation of NO on Pt to form NO_2, which desorbs and stores on BaO. The second is by spillover of adsorbed NO_2 and/or NO and O from Pt to BaO via the Pt/BaO interface. There was no evidence for gaseous NO_2 formation during the NO pulsing experiments based on the absence of the $m/e = 46$ peak. In a series of experiments (not reported here) that involved NO_2 pulsing over the Pt/Al_2O_3 catalyst in the temperature range 200–400 °C, NO_2 readily decomposed forming NO, O_2 and N_2. In the current NO pulsing experiments, O_2 was not observed in the effluent. Thus, the possibility of formation of gaseous NO_2 as product is ruled out. However, this does not rule out the formation of adsorbed NO_2, which may spillover from the Pt to BaO. Indeed, the results suggest that NO_X spillover is the major mechanism for NO_X storage. The reaction network of NO decomposition, NO_X storage and reduction on Pt/Al_2O_3 and $Pt/BaO/Al_2O_3$ is discussed in our earlier work [13,14].

In order to determine the contribution of Pt in the storage process, the NO (or ^{15}NO) storage experiment was repeated at 350 °C over the BaO/Al_2O_3 sample. The stored N was about 2×10^{-6} moles N/g; this value is less than 5% of the storage on the $Pt/BaO/Al_2O_3$ sample for the same NO exposure at that temperature. This underscores the importance of Pt during NO_X uptake. Post-storage reduction using H_2 was not able to reduce the stored NO_X, but a temperature programmed desorption (TPD) was able to remove the small amount of NO_X present on the BaO/Al_2O_3. These results are consistent with the negligible NO storage on BaO/Al_2O_3 during bench scale studies reported by Nova et al. [22] under atmospheric pressure conditions. To lend further support, atmospheric experiments (not reported here) in our laboratory reveal that NO_2 can readily adsorb on BaO/Al_2O_3 but the reduction with H_2 does not take place in absence of Pt. These observations imply that Pt serves as a conduit for NO_X storage (transport of NO_X from gas phase to Pt to BaO) and NO_X reduction (transport of NO_X from BaO to Pt followed by reduction). The transport of NO_X species from Pt to BaO or vice versa takes place through the Pt/BaO interface. Since BaO alone does not participate in either NO_X storage or removal, spillover processes are crucial during NSR especially involving sites at the vicinity of the Pt/BaO interface.

3.2. NO–^{15}NO isotopic exchange

Isotopic exchange experiments were carried out on the Pt/BaO/Al_2O_3 and BaO/Al_2O_3 samples that would help in interpreting NO_X reduction experiments later. In particular, the exchange measurements help to elucidate the involvement of the Pt/BaO interface and mobility of NO_X species during isotopic exchange. Experimental data are reported below in which ^{15}NO desorption was monitored from pre-nitrated catalyst in the presence and absence of NO pulses. In a typical experiment, the Pt/BaO/Al_2O_3 and BaO/Al_2O_3 catalysts were pre-nitrated with 1500 pulses of ^{15}NO at 350 °C. The pre-nitrations were then followed by two types of independent experiments described next.

3.2.1. ^{15}NO desorption in absence of NO pulsing

^{15}NO was allowed to desorb from the pre-nitrated Pt/BaO/Al_2O_3 in the absence of gaseous pulses. The results are shown in Fig. 2. The ^{15}NO desorption profiles are identical to those obtained when the desorption takes place during Ar pulsing. Similar experiments of ^{15}NO storage followed by desorption were repeated for the BaO/Al_2O_3 catalyst, but the desorption was insignificant in the absence of Pt.

3.2.2. ^{15}NO desorption during NO pulsing

NO pulsing on Pt/BaO/Al_2O_3 that was pre-nitrated with 1500 pulses of ^{15}NO at 350 °C resulted in a significant exchange of stored ^{15}NO by fed NO. Using the method described earlier, 2.7×10^{18} ^{15}N atoms have been stored on the catalyst during the initial 1500 pulses of ^{15}NO. Fig. 2 shows the results when the pre-nitrated (with ^{15}NO) Pt/BaO/Al_2O_3 sample was then exposed to a sequence of unlabeled NO pulses containing 8.7×10^{15} molecules/pulse on average. A fraction of the NO pulsed during the initial pulses was stored on Pt/BaO/Al_2O_3 while the rest exited the reactor. ^{15}NO desorbed from the pre-nitrated Pt/BaO/Al_2O_3 and was also detected in the effluent. The amount of ^{15}NO left on the catalyst decreased with time and the corresponding exit flux of ^{15}NO decreased monotonically.

The amount of ^{15}NO removed from the catalyst during the first 100 NO pulses exceeds the number of exposed Pt sites. This indicates that the exchange of ^{15}NO by NO does not take place on Pt alone but must also involve NO_X stored in the barium phase. The isotopic exchange data suggest that exposure of NO to pre-nitrated (using ^{15}NO) Pt/BaO/Al_2O_3 results in the transport of NO_X species from Pt to BaO and $^{15}NO_X$ species from BaO to Pt, both processes occurring via the Pt/BaO interface. Stored $^{15}NO_X$ diffuses from the storage phase to the Pt/BaO interface where it spills over and then desorbs. There is clearly some mobility of NO_X species in the barium phase as well as across the Pt/BaO interface [21]. The ^{15}NO storage followed by the NO–^{15}NO isotopic exchange experiment was repeated on BaO/Al_2O_3, but the ^{15}NO desorption was insignificant in the absence of Pt.

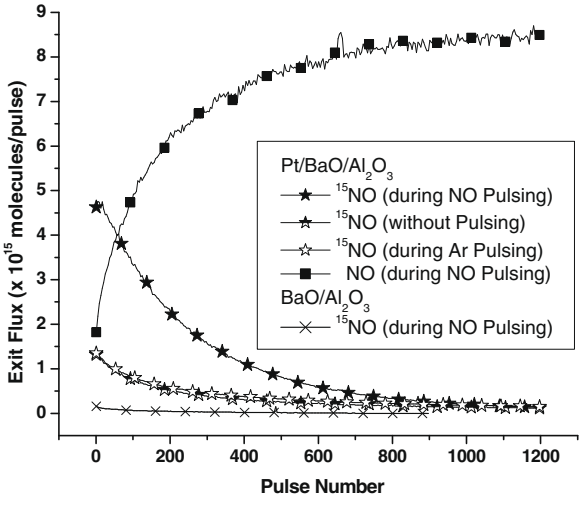

Fig. 2. Isotopic exchange of ^{15}NO by unlabeled NO and effect of NO pulsing, without pulsing and Ar pulsing on ^{15}NO desorption from pre-nitrated (using ^{15}NO) Pt/BaO/Al_2O_3 and BaO/Al_2O_3.

A comparison of ^{15}NO storage and NO–^{15}NO isotopic exchange over Pt/BaO/Al_2O_3 and BaO/Al_2O_3 highlights the importance of Pt and the processes occurring at the Pt/BaO interface. ^{15}NO storage is negligible in the absence of Pt, and NO pulsing on pre-nitrated BaO/Al_2O_3 (using ^{15}NO) resulted in negligible exchange of ^{15}NO by NO. Thus, BaO alone does not take part in either NO storage or NO–^{15}NO exchange. Rather, NO and ^{15}NO exchange takes place via the Pt/BaO interface through spillover processes.

A comparison of the exit flux of ^{15}NO in the presence and absence of NO pulses indicates that NO enhances the ^{15}NO removal from the catalyst. In the absence of NO pulses, ^{15}NO desorbs from the catalyst, creating vacant sites on the Pt. The desorbed ^{15}NO can re-adsorb on the vacant sites freed up by the desorbing ^{15}NO. In contrast, in the presence of the NO pulses, vacant sites created by ^{15}NO desorption are filled by the pulsed NO. The presence of NO likely does not increase the desorption rate of ^{15}NO from the catalyst, but it does inhibit the re-adsorption of ^{15}NO. This results in an enhancement of ^{15}NO removal from the catalyst in the presence of NO. The sequential desorption and re-adsorption of ^{15}NO in the absence of NO cause the overall ^{15}NO removal rate to be lower than that during NO-assisted ^{15}NO removal.

These isotopic exchange experiments suggest that a gradient in labeled (or unlabeled) NO_X can be created in the storage phase of the Pt/BaO catalyst. $^{15}NO_X$ storage occurs in the vicinity of the Pt/BaO interface. This leads to a stored $^{15}NO_X$ concentration that decreases from the Pt/BaO interface into the bulk storage phase. Subsequent pulses of unlabeled NO adsorb on Pt and isotopic exchange readily occur via the Pt/BaO interface. The magnitude of the gradient in $^{15}NO_X$ concentration is determined by its mobility. In the limit of rapid mobility, the stored NO_X would lead to a uniform concentration of stored labeled and unlabeled NO_X species. However, as we show later, the finite mobility results in a gradient within the storage phase.

3.3. ^{15}NO–H_2 pump–probe on pre-nitrated (using unlabeled NO) Pt/BaO/Al_2O_3

Isotopic pump–probe experiments provide evidence for N_2 formation on Pt and for spillover processes during NSR. The catalyst was pre-nitrated using 1500 pulses (pulse size = 2.0×10^{16} molecules/pulse) of unlabeled NO at 250 °C. About 4.4×10^{18} molecules of N were stored during this pre-nitration. About 8 min after pre-nitration (i.e. time taken to purge NO from gas line and fill it with H_2), sequential pulses of ^{15}NO and H_2 were fed to the pre-nitrated (using NO) Pt/BaO/Al_2O_3 catalyst. The delay between successive ^{15}NO and H_2 pulses in a single pump–probe cycle was kept at 4 s, and the spacing between successive H_2 and ^{15}NO pulses was also kept at 4 s. A longer spacing time (>4 s) would lead to desorption of NO from the catalyst. During each cycle, ^{15}NO was pulsed at the 0th s and then H_2 was pulsed at the 4th s (Fig. 3). This cycle was repeated after every 8.0 s. The ratio of H_2 to ^{15}NO fed to the reactor was maintained in excess of H_2 ($H_2/^{15}NO = 3.9$), conditions for which NO conversion is complete [13,14]. The absence of gaseous NO during these excess H_2 conditions ensures that the $m/e = 30$ signal is solely attributed to $^{15}N_2$.

The data reveal the production of three types of nitrogen (N_2, $^{15}N_2$ and ^{15}NN) and NH_3 during the ^{15}NO and H_2 pulses over

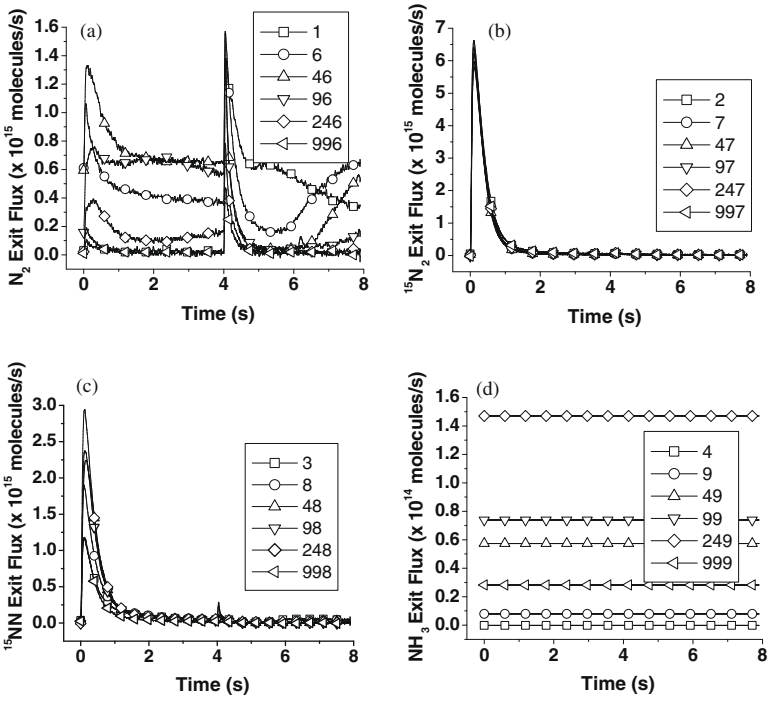

Fig. 3. Individual transient profiles of N_2 (a), $^{15}N_2$ (b), ^{15}NN (c) and NH_3 (d) during ^{15}NO–H_2 pump–probe on pre-nitrated (using unlabeled NO) $Pt/BaO/Al_2O_3$ at 250 °C. ^{15}NO was pulsed at 0th s, and H_2 was pulsed at 4th s. Legends are ^{15}NO–H_2 cycle numbers.

1000 full cycles (Figs. 3 and 4). The formation of $^{15}N_2$ is evident from the outset and was sustained throughout the experiment, but it appeared only during the ^{15}NO pulse (Fig. 3b). The individual transient flux response of $^{15}N_2$ pulse was in the form of a sharp peak followed by a rapid decay. This profile resembles that for N_2 produced during the NO pulsing experiment on pre-reduced Pt/Al_2O_3 [13,14] or $Pt/BaO/Al_2O_3$ [13]. Those studies attributed the nitrogen formation to NO decomposition due to the effective removal of surface oxygen by the pulsed H_2. Similarly, in the current study, the H_2 pulse following each ^{15}NO pulse served to scavenge oxygen left on Pt sites by ^{15}NO decomposition.

The second type of nitrogen formed during this experiment was ^{15}NN, which we refer as mixed isotopic nitrogen (Fig. 3c). It was almost exclusively formed during the ^{15}NO pulse and is attributed to the following chemistry. ^{15}NO bond scission occurs on reduced Pt, generating ^{15}N adatoms. In addition to the recombination of two ^{15}N adatoms (to form $^{15}N_2$), recombination of ^{15}N and N may occur, forming ^{15}NN. The individual transient response of ^{15}NN was also in the form of a sharp peak followed by a rapid decay. Its similarity to the $^{15}N_2$ effluent peak suggests that the primary route for formation of ^{15}NN is from ^{15}NO decomposition followed by combination of N and ^{15}N. The only difference is the source of the N adatoms. Rather than coming from the gas phase, the main source of the unlabeled N is from the barium nitrite/nitrate phase. A negligible but non-zero peak of ^{15}NN was also observed during H_2 pulsing. Its existence suggests that additional nitrogen formation occurs via chemistry occurring at the Pt/BaO interface. The production of ^{15}NN is direct evidence of a reverse spillover process from the Ba storage phase to Pt. More conclusive evidence of this pathway is the formation of unlabeled N_2, as we discuss in more detail later. Eventually, as the stored unlabeled NO_X depletes, the formation of ^{15}NN also declines at the expense of an increase in $^{15}N_2$. The integral response of ^{15}NN indicates that a small but non-zero production of ^{15}NN occurs during initial cycles, which increases to a plateau between the 50th and 250th cycles (Fig. 4). The initial increasing trend indicates that as H_2 removes the O from the Pt surface, this promotes the decomposition of stored, unlabeled NO_X, leading to an increase in formation of ^{15}NN.

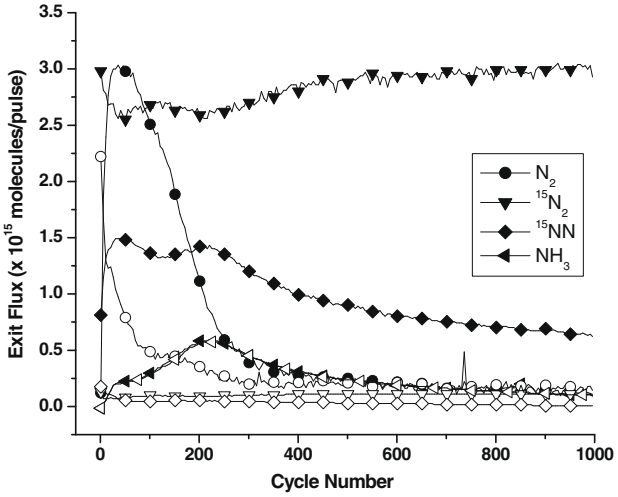

Fig. 4. N_2, $^{15}N_2$, ^{15}NN and NH_3 integral profiles during ^{15}NO pulse (solid symbols) – H_2 pulse (open symbols) 1000 pump–probe cycles ($H_2/^{15}NO = 3.9$) on pre-nitrated (with NO) $Pt/BaO/Al_2O_3$ at 250 °C.

The formation of unlabeled N_2 exhibited complex behavior throughout the 1000 pump–probe cycle experiment (Fig. 3a). N_2 was not observed during the first ^{15}NO pulse on the pre-nitrated (with NO) catalyst. However, the subsequent H_2 pulse resulted in a sharp increase in N_2 formation. This suggests that H_2 scavenges O adatoms, freeing up sites for the catalytic decomposition and/or reduction of stored unlabeled NO_X. The data reveal that the 4 s spacing between the H_2 pulse and next ^{15}NO pulse is not of sufficient duration for the N_2 signal to return to the baseline level. The N_2 baseline slowly increased during subsequent ^{15}NO pulses

(see pulse 6th, 46th etc.) and then eventually decreased (see pulse 96th, 246th etc.). The N_2 signal during the ^{15}NO pulses has distinct peaks as does the N_2 signal during the H_2 pulses, which are even sharper. It is noted that the N_2 signal slowly increased 1–2 s after its initial peak during the H_2 pulse. This feature is more prominent earlier in the 1000-cycle experiment. The increased signal carries forward during subsequent ^{15}NO pulses resulting in larger N_2 production during the ^{15}NO pulse than H_2 pulse. As stored unlabeled NO_X gets depleted, the peak N_2 signal gradually decreased throughout the course of the experiment.

The integral N_2 profile has a maximum at the first H_2 pulse, but a negligible value during the ^{15}NO pulse (Fig. 4). Subsequent cycles show a monotonic decrease in the N_2 intensity during the H_2 pulse. In contrast, the N_2 signal during the ^{15}NO pulses increases sharply and exhibits a maximum at the 36th cycle. The decrease after 36th cycle suggests that N_2 is produced by reaction of stored NO_X species with H_2, but as the stored species get depleted, the production of N_2 decreases.

The excess H_2 readily reacts with adsorbed N and O on Pt to form NH_3 and H_2O, respectively, creating vacant Pt sites for further adsorption and reaction [25]. The transient formation of NH_3 is indicated by the increasing baseline signal rather than a distinct peak (Fig. 3d). Its appearance in the reactor effluent being gradual but continuous suggests its slow desorption from the catalyst. In fact, the integral profiles of NH_3 are identical during the ^{15}NO and H_2 pulses (Fig. 4). The NH_3 formation profiles increase from zero during the initial cycles, achieve respective maxima at about the 230th cycle and then slowly decline as the stored NO_X is depleted. Labeled ammonia ($^{15}NH_3$) was not measured due to its overlap with H_2O (i.e. peaks at $m/e = 18$ and 17). However, based on our earlier study using $NO–H_2$ pump–probe over Pt/Al_2O_3 [14], delay times shorter than 0.1 s resulted in significant ammonia formation while delay times longer than 1 s led to negligible ammonia. Thus, $^{15}NH_3$ formation is expected to be negligible in these experiments having a $^{15}NO–H_2$ delay of 4 s.

These findings show that the formation of N_2 occurs on Pt with active participation of the barium storage phase. The uptake of unlabeled N and O during the pre-nitration followed by the $^{15}NO–H_2$ pump–probe cycles results in the formation of unlabeled N_2 and the mixed product ^{15}NN. At the lower temperature of 250 °C, the non-catalytic decomposition of nitrate or nitrite is negligible [26]. It is also known that the reduction of stored NO_X on BaO/Al_2O_3 in the absence of Pt in both the vacuum conditions of the TAP and the atmospheric conditions of a bench flow reactor does not occur.

In order to further understand the involvement of NH_3 to produce N_2, we performed an independent NH_3 uptake experiment over Pt/Al_2O_3 catalyst at 250 °C. Ammonia was fed to the reactor during 0–1500 pulses. At 1500th pulse, the pulsing was stopped and it was allowed to desorb isothermally. The inlet pulse size of NH_3 was 5.3×10^{16} molecules/pulse, while the spacing time between consecutive NH_3 pulses was kept 12 s. The individual pulse profiles were similar to that plotted in Fig. 3d, indicate that even though the inlet NH_3 fed to the reactor was in the form of sharp pulses but the evolution of NH_3 in the effluent is continuous. The above data suggest a rapid adsorption of gaseous NH_3 on the catalyst and slow desorption of adsorbed NH_3 from the catalyst. Moreover, the NH_3 adsorption during first 200 pulses (Fig. 5) was ca. 6.0×10^{18}, which is five times larger than exposed Pt sites (1.2×10^{18}), indicating that NH_3 adsorbs not only on exposed Pt sites but also on exposed alumina and may be on reactor walls, mass spectrometer surface and inert glass beads. A comparative exposed area of the alumina (~10 m^2), Pt (~0.1 m^2), reactor surfaces including mass spectrometer (0.1 m^2) and glass beads (0.01 m^2) suggests that prominent adsorption/desorption can be attributed to exposed alumina due to its high surface area and

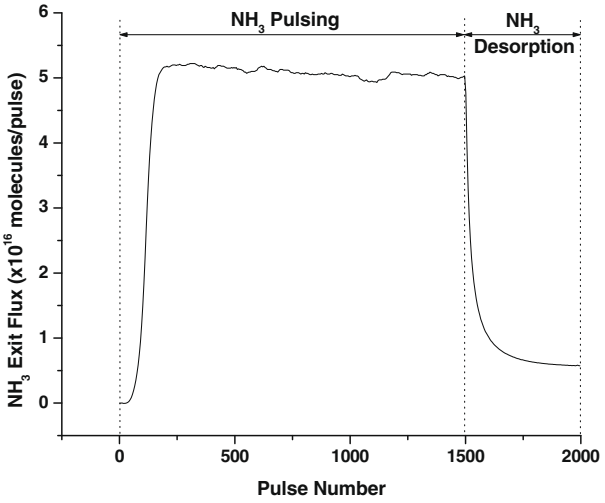

Fig. 5. Integral NH_3 effluent profiles during NH_3 pulsing (1–1500 pulse) followed by desorption (1501–2000 pulse) over Pt/Al_2O_3 catalyst at 250 °C.

acidic nature. The subsequent desorption at 250 °C during 1501–2000 pulses highlights slow and continuous desorption from the catalyst.

The transient production of molecular nitrogen during the pump–probe experiment occurs by either a distinct peak or a rising baseline. The peak-like formation of $^{15}N_2$ is clearly a result of the decomposition of ^{15}NO on clean Pt. This is also the case for ^{15}NN, with the minor difference being that recombination of ^{15}N adatoms from gas phase ^{15}NO and N from stored NO_X occurs. Apart from these, the peak-like formation of N_2 during H_2 pulse confirms the scavenging role of H_2 to form water, whose desorption creates vacant sites for stored NO_X decomposition in the proximity of Pt/BaO interface to form N_2. In addition, during ^{15}NO pulse, adsorbed NH_X ($x = 1$, 2 or 3) react with surface ^{15}NO to form ^{15}NN and H_2O, which indeed creates vacant sites for interfacial NO_X decomposition to form N_2 and peak-like N_2 formation appears. In contrast to peak-like nitrogen formation, the rising baseline evident during N_2 formation suggests the reaction of H_2 with NO_{ad} and/or N_{ad} to form NH_3, which can desorb, re-adsorb and react with NO_{ad}, forming N_2. These processes lead to the delay in appearance of NH_3 in the effluent and, when it finally appears, the rising baseline feature emerges. This feature, emulated by the changing baseline signal of N_2, provides strong evidence for the N_2 formation via the NH_3 intermediate. The formation of NH_3 as an intermediate during NO_X reduction over $Pt/BaO/Al_2O_3$ using H_2 is by now well established [27–29].

The integral exit flux for NH_3 (Fig. 4) first increases and then eventually decreases due to the depletion of stored unlabeled NO_X. This suggests that NH_3 is produced in significant amounts during the initial pulses but is not seen in the reactor exit because of its reaction with stored NO_X, forming N_2. Thus, there are two reductants, H_2 and NH_3 that are in competition to reduce stored NO_X. At the end of the NO storage treatment, the amount of stored NO_X is at its highest level. The data indicate that both H_2 and NH_3 are effective in reducing NO_X to N_2 during the initial H_2 pulses. As the experiment progresses, the stored, unlabeled NO_X depletes. As a result, the formation of NH_3 declines. The competition between H_2 and NH_3 in reducing the depleting supply of stored NO_X leads to lower NH_3 conversion, and as a result, unreacted NH_3 in the reactor effluent starts to increase. At about the 230th cycle number, the NH_3 observed in reactor effluent reaches a maximum and eventually starts to decrease due to the depletion of stored unlabeled NO_X.

3.4. ^{15}NO pulsing followed by reduction on pre-nitrated (using unlabeled NO) $Pt/BaO/Al_2O_3$

In order to further our understanding of the NO_X spillover from Pt to BaO, reverse spillover from BaO to Pt, and distribution of stored NO_X in the barium phase, a sequential storage of NO followed by ^{15}NO and reduction by H_2 was carried out over $Pt/BaO/Al_2O_3$ at 300 °C. The spacing between two consecutive pulses was maintained at 4.0 s during the pre-nitrations (with NO, ^{15}NO) and reduction. The catalyst was pre-nitrated using 1500 pulses (pulse size = 1.11×10^{16} molecules/pulse) of unlabeled NO at 300 °C. About 4.1×10^{18} molecules of N were stored on the catalyst during the pre-nitration. This was followed by the sequential storage of ^{15}NO for 90 pulses on the pre-nitrated $Pt/BaO/Al_2O_3$. The pulses of ^{15}NO on pre-nitrated catalyst resulted in the isotopic exchange of NO with ^{15}NO and an additional storage as shown during the first 90 pulses (Fig. 6). By monitoring the effluent composition, the ratio of stored N to stored ^{15}N on the catalyst was estimated to be 5.3 by the end of ^{15}NO exposure.

The pre-nitrations were followed by reduction with H_2 during pulses 91–600 at the same temperature. The reduction resulted in the formation of three types of nitrogen (N_2, $^{15}N_2$ and ^{15}NN) and two types of ammonia (NH_3 and $^{15}NH_3$), in addition to H_2O and unreacted H_2. The excess of H_2 enabled complete consumption of NO (m/e = 30) and ^{15}NO (m/e = 31) so that these species were not observed in the reactor effluent. Thus, the signal of m/e = 30 was exclusively from $^{15}N_2$. (Comment: if temperature programmed desorption (TPD) was carried out instead of reduction, the effluent would contain both NO and $^{15}N_2$ and it would have been impossible to distinguish between them.) At the 601st pulse, the temperature programmed surface reaction (TPSR) was performed during the pulsing of H_2. At the end of the TPSR, the temperature of the catalyst was 420 °C.

As before, H_2O and $^{15}NH_3$ were not measured during the experiment due to the overlapping signals at m/e = 18 and 17. In order to estimate the $^{15}NH_3$ during this experiment, a similar but non-isotopic experiment of 90 unlabeled NO pulses on pre-nitrated (with 1500 NO pulses) catalyst followed by reduction with H_2 was performed. The pulse sizes were kept nearly identical to the earlier experiment. The reduction resulted in the formation of N_2, NH_3 and H_2O, but no isotopic species. Thus, the NH_3 in this non-isotopic experiment would be equivalent to the combined NH_3 and $^{15}NH_3$ signals in the earlier isotopic experiment. The amount of $^{15}NH_3$ during the isotopic experiment, which was not measured, was estimated by the difference of NH_3 in non-isotopic and isotopic experiments.

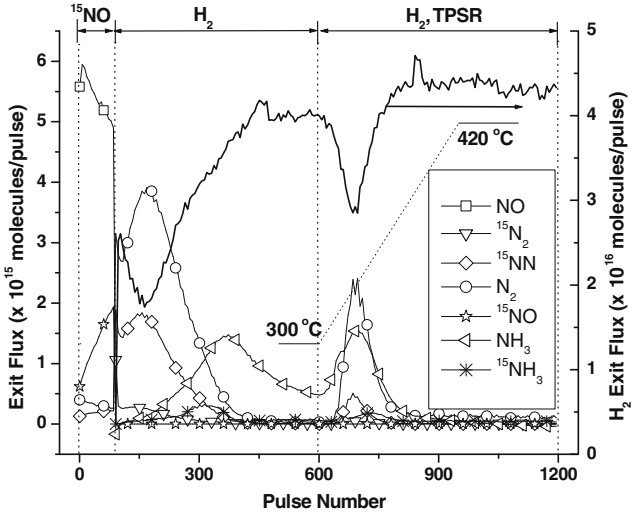

Fig. 6. ^{15}NO pulsing followed by reduction at 350 °C and TPSR over a pre-nitrated (using unlabeled NO) $Pt/BaO/Al_2O_3$.

The results reveal similar integral trends for N_2, $^{15}N_2$ and ^{15}NN during reduction but with different magnitudes of the effluent fluxes. Table 2 compares the magnitudes of the three forms of nitrogen evolved during the H_2 exposure for pulses 91–600 and temperature programmed surface reaction (TPSR) for pulses 601–1200. The unlabeled N_2 and mixed isotopic ^{15}NN were the main products while $^{15}N_2$ was the minor product. The data show that the integral profiles of three types of nitrogen declined with pulse number as the stored N and ^{15}N were consumed during the reduction (Fig. 6). In addition to the three types of molecular nitrogen, NH_3 and $^{15}NH_3$ were also observed. NH_3 was not seen in the reactor exit during the initial H_2 pulses, but its production increased to a maximum and eventually decreased due to the depletion of stored NO_X. The formation of $^{15}NH_3$ followed similar trends but its magnitude was much lower than that of NH_3. A temperature ramp at the 601st pulse resulted in an increased production of N_2, ^{15}NN and NH_3 at the expense of increased consumption of H_2. Eventually, as the pulsing continued, the effluent N- and ^{15}N-containing species declined due to the depletion of the stored N and ^{15}N species.

The effluent fluxes of $^{15}N_2$, ^{15}NN and N_2 during reduction depend on the extent of pre-nitration of the $Pt/BaO/Al_2O_3$ catalyst with NO and ^{15}NO. A fixed NO exposure (1500 pulses) followed by the smaller number of ^{15}NO pulses (90 pulses) and then reduction resulted in a larger flux of unlabeled N_2 (Fig. 6). In separate reduction experiments (not reported here) with a similar NO exposure during a pre-nitration step followed by a large number of ^{15}NO pulses resulted in a larger effluent flux of $^{15}N_2$. However, reduction followed by an intermediate number of ^{15}NO pulses resulted in larger fluxes of ^{15}NN and smaller $^{15}N_2$ and N_2 during post-nitration reduction.

In order to quantify the amount of N and ^{15}N in the effluent during reduction, the following overall mole balances were used:

$$N^{Effluent} = (NO + {}^{15}NN + 2N_2 + NH_3)^{Effluent} \quad (4)$$

$$^{15}N^{Effluent} = (^{15}NO + {}^{15}NN + 2{}^{15}N_2 + {}^{15}NH_3)^{Effluent} \quad (5)$$

Combining Eqs. (4) and (5) gives,

$$\left(\frac{N}{^{15}N}\right)^{Effluent} = \left(\frac{NO + {}^{15}NN + 2N_2 + NH_3}{^{15}NO + {}^{15}NN + 2{}^{15}N_2 + {}^{15}NH_3}\right)^{Effluent} \quad (6)$$

Eq. (6) gives the ratio of N to ^{15}N in the effluent based on the measured effluent fluxes. Note that, adsorption, desorption and re-adsorption features may delay the appearance of ammonia in the effluent, which can cause some error in the estimation of ratios. Using Eq. (6), the instantaneous $N/^{15}N$ ratio during nth pulse, $(N/^{15}N)_{I,n}$, in the reactor effluent can be estimated from the exit fluxes of the nth pulse; i.e.

$$\left(\frac{N}{^{15}N}\right)_{I,n}^{Effluent} = \left(\frac{NO + {}^{15}NN + 2N_2 + NH_3}{^{15}NO + {}^{15}NN + 2{}^{15}N_2 + {}^{15}NH_3}\right)_{n}^{Effluent}, \quad 1 \leqslant n \leqslant 1200 \quad (7)$$

As shown in Fig. 6, at the first pulse of ^{15}NO on the pre-nitrated (using NO) catalyst, most of the effluent consisted of NO. Eq. (7) gives $(N/^{15}N)_I \sim 8.7$ (Fig. 7). As the exposure of ^{15}NO increased,

Table 2
Amount of three isotopes of molecular nitrogen during H_2 pulsing.

Species	Number of molecules (pulse 91–600), T = 300 °C	Number of molecules (pulse 601–1200), T = 300–420 °C
$^{15}N_2$	4.8×10^{16}	7.9×10^{15}
^{15}NN	2.9×10^{17}	3.0×10^{16}
N_2	6.9×10^{17}	2.3×10^{17}

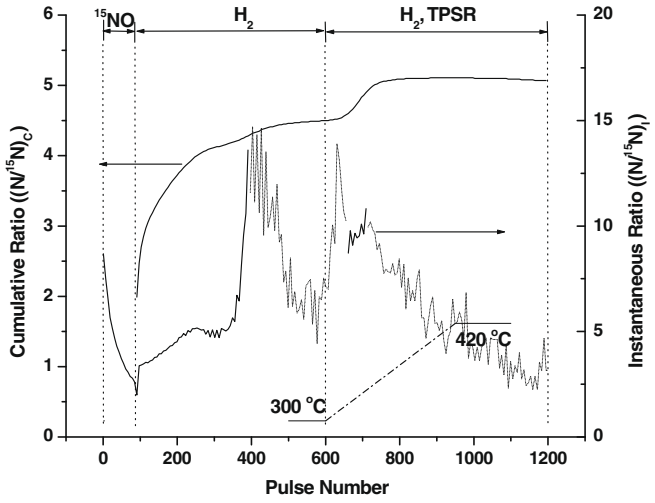

Fig. 7. Instantaneous and cumulative N/^{15}N ratio during ^{15}NO and H_2 pulsing on pre-nitrated (using unlabeled NO) Pt/BaO/Al_2O_3 at 300 °C. The dotted lines for instantaneous ratio represent below detection limit ^{15}N-containing flux that causes larger fluctuations and erroneous ratio.

the desorbing NO decreased due to the depletion of stored unlabeled NO_X (Fig. 6). In turn, the non-adsorbing ^{15}NO present in the reactor effluent increased. These processes resulted in a decrease in $(N/^{15}N)_I$ value from 8.7 to 2.0 during the 90 pulses of ^{15}NO exposure. By the 90th pulse, the amount of stored N and ^{15}N on the catalyst is estimated to be 3.5×10^{18} and 6.6×10^{17}, respectively, and the corresponding ratio of stored N to ^{15}N was 5.3.

The NO and ^{15}NO pre-nitrations were followed by reduction at 300 °C in H_2. In addition to $(N/^{15}N)_I$, the cumulative N/^{15}N ratio at the reactor exit, $(N/^{15}N)_C$, was also estimated during the reduction. $(N/^{15}N)_{C,n}$ at the nth pulse is defined as the ratio of total N to ^{15}N produced between the 91st and nth pulse (Eq. (8)):

$$\left(\frac{N}{^{15}N}\right)_{C,n}^{\text{Effluent}} = \frac{\sum_{j=91}^{n}(NO + {}^{15}NN + 2N_2 + NH_3)_j^{\text{Effluent}}}{\sum_{j=91}^{n}({}^{15}NO + {}^{15}NN + 2{}^{15}N_2 + {}^{15}NH_3)_j^{\text{Effluent}}}, \quad 91 \leqslant n \leqslant 1200 \tag{8}$$

At the start of reduction (i.e. at the 91st pulse), the formation of nitric oxide (NO, ^{15}NO) decreased to zero while nitrogen (N_2, $^{15}N_2$, ^{15}NN) formation sharply increased. In turn, $(N/^{15}N)_I$ increased from 2.0 to 14 while $(N/^{15}N)_C$ steadily increased from 2.0 to 4.3 during 91–400 pulse interval. After 400 pulses, the formation of ^{15}N-containing species approached the baseline level, which resulted in larger fluctuations in the $(N/^{15}N)_I$ ratio. On the other hand, $(N/^{15}N)_C$ slowly increased to 4.5 at the end of 600th pulse.

At the 601st pulse, the temperature was ramped to 420 °C with a ramp rate of 15 °C/min. As the temperature increased, the formation of N_2 and NH_3 increased sharply. In addition to N-containing species, a relatively small but non-zero production of ^{15}NN was also observed. This led to an increase in the cumulative ratio, $(N/^{15}N)_C$ to 5.1 by the end of 1200th pulse, which is closer to the ratio of stored N to ^{15}N (=5.3) just before the beginning of the reduction, i.e. at the 90th pulse.

Thus, the initial H_2 pulses (91–300) preferentially removed ^{15}N-containing species ($^{15}N_2$, ^{15}NN and $^{15}NH_3$) from the Pt/BaO/Al_2O_3 sample, which had been pre-nitrated first with NO followed by ^{15}NO. The preference of evolution shifted toward N-containing species (N_2, ^{15}NN and NH_3) during later reduction pulses (300–1200). These results indicate that the pre-nitration with NO results in NO_X storage in the vicinity of Pt in the barium phase. The subsequent nitration with ^{15}NO leads to some exchange of NO_X by $^{15}NO_X$ in the proximity of Pt/BaO interface. The regeneration data suggest the existence of a gradient of stored NO_X and $^{15}NO_X$ in the barium phase. Had the storage of unlabeled and labeled NO_X been uniform, then the reduction would have resulted in a constant values of the instantaneous ratio $(N/^{15}N)_I$ and cumulative ratio $(N/^{15}N)_C$. That constant ratio would be equal to the ratio of stored N to ^{15}N just before the reduction, i.e. 5.3. But an increase in $(N/^{15}N)_I$ from 2.0 to 14 and $(N/^{15}N)_C$ from 2.0 to 5.1 during pulses 91–1200 rules out the existence of a "well-mixed" phase containing labeled and unlabeled NO_X. Rather, the result suggests that there are radial gradients of stored ^{15}N and N species on the barium phase.

Clayton et al. [30] compared storage and reduction rates for catalysts with 3.2%, 8% and 50% Pt dispersion, having the same Pt and BaO loadings. They concluded that the regeneration rate of the 3.2% dispersion catalyst was much slower due to a transport limitation of stored NO_X from BaO phase to the Pt/BaO interface. This feature has been confirmed in the modeling studies by Bhatia et al. [31]. In the current TAP experiment, the reduction was not feed limited as the H_2 was detected in the effluent during the reduction process. This suggests that the regeneration is limited by the transport of stored NO_X, by either surface and/or solid state diffusion, from the BaO storage phase to the Pt/BaO interface. Moreover, as the temperature of the catalyst is increased, the transport rates of stored NO_X also increased, resulting in the increased reduction of stored NO_X at the Pt/BaO interface (Fig. 6). Catalyst temperatures exceeding 400 °C further increases the stored NO_X transport rate but at these temperatures, decomposition of stored NO_X may also occur.

It is instructive to speculate how these findings might affect the surface concentration profiles of stored NO_X. Fig. 8 shows a schematic of the concentration distributions of labeled and unlabeled stored NO_X in the form of nitrates throughout the course of the storage and reduction experiment. Fig. 9 provides a corresponding set of concentration profiles. As depicted in Figs. 8b and 9a, pre-nitration using NO leads to a radial gradient in stored unlabeled NO_X that decreases with distance from the Pt/BaO interface. An increase in the exposure of NO expands the region over which stored NO_X resides. During subsequent exposure to ^{15}NO, the stored N is exchanged by ^{15}N in the proximal region of the Pt/BaO interface. As in the case of the unlabeled NO_X after the exposure to NO, the concentration of stored ^{15}N declines radially with distance from the Pt/BaO interface (Figs. 8c and 9c). Moreover, since NO and ^{15}NO have similar chemical properties, the combined N and ^{15}N concentration decreases radially away from the Pt/BaO interface.

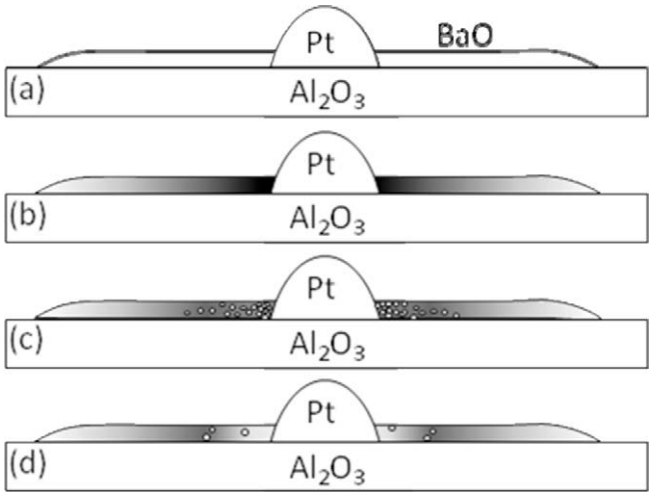

Fig. 8. Schematic diagram of stored NO_X (shade) and $^{15}NO_X$ (dots) concentration distribution in barium: (a) pre-reduced catalyst, (b) NO storage, (c) ^{15}NO–NO isotopic exchange and (d) reduction.

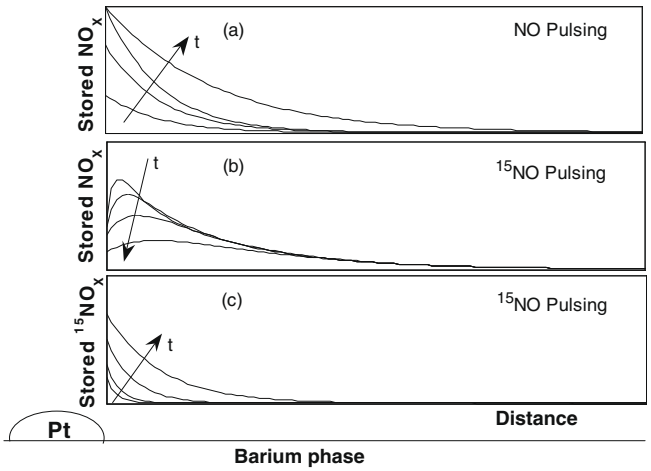

Fig. 9. Schematic profiles for labeled and unlabeled NO_X storage in the barium phase.

However, the exchange of N with ^{15}N results in an N profile that has a local maximum (Fig. 9b). During reduction, depletion of stored NO_X occurs in the proximity of the Pt/BaO interface. With the reduction being transport limited, the stored NO_X concentration in the stored phase increases with distance from the Pt/BaO interface, attains a maximum and declines monotonically (Fig. 8d).

It should be pointed out that the low Pt dispersion (3.2%) catalyst was selected for this study as our parallel bench scale experiments at 1 atm showed clearly that some transport limitations at the crystallite level (and not external mass transfer or washcoat diffusional limitations) may be responsible for the slow regeneration of the stored NO_X [30]. In contrast, the regeneration of the NO_X for the case of high Pt dispersion (50%) catalyst was found to be much faster and feed rate limited. One possible reason for this is that for the high dispersion case, the average distance between the stored NO_X and Pt/BaO interface is much smaller compared to the low dispersion case. Thus, the radial gradients, if they exist, may be much smaller for the high dispersion case. Also, in the low dispersion case, when the amount of stored NO_X is small, most of the storage occurs in the proximity of the Pt/BaO interface. Hence, the radial gradients may not be important, e.g. if we used only 100 pulses of NO (instead of 1500 pulses) followed by similar ^{15}NO exposure (90 pulses), the radial gradients are expected to be much smaller as most of the NO_X is stored near the Pt/BaO interface. Crystallite level modeling may be used to quantify the magnitude of the radial gradients in terms of the Pt dispersion/loading, BaO loading and the amount of NO_X stored. This complementary modeling study is ongoing and will be presented elsewhere.

In real practical automobile application, the Pt dispersion is much higher than used in this study. The diffusional transport limited reduction of stored NO_X is more realistic during low temperature NO_X reduction e.g. during conditions of cold start of engine. Moreover, the prolong operation and severe temperature conditions of catalytic monolith lead to sintering of the Pt and hence dispersion of the Pt decreases. The transport limited conditions are more realistic at lower Pt dispersion case, and it shifts to feed limited conditions at high dispersion.

4. Conclusions

We have carried out isotopically labeled storage and reduction over $Pt/BaO/Al_2O_3$ in the TAP reactor system to elucidate the role of spillover processes and Pt/BaO interface during NO_X storage and reduction. The BaO/Al_2O_3 in the absence of Pt does not participate in either storage of NO or reduction of stored NO_X by H_2. Pt serves as a conduit for adsorption and reaction as well as spillover to and from the barium phase. The NO_X species spills over from Pt to barium via Pt/BaO interface during the storage cycle and the NO_X species spills back from BaO to Pt during reduction.

The sequential pre-nitration of $Pt/BaO/Al_2O_3$ using NO and ^{15}NO followed by reduction with H_2 results in the preferential evolution of ^{15}N-containing species during initial H_2 pulses. The evolution shifts toward unlabeled N-containing species in later H_2 pulses. The data suggest that NO_X storage proceeds radially outward from Pt crystallites and that some mobility of the stored NO_X species exists. The subsequent reduction is limited by transport of stored NO_X from BaO storage phase to the Pt/BaO interface.

The evolution of N_2 and ^{15}NN during $^{15}NO–H_2$ pump–probe on pre-nitrated (using unlabeled NO) catalyst confirms the involvement of spillover processes at the Pt/BaO interface. A sequential pulsing of $^{15}NO–H_2$ pump–probe on pre-nitrated catalyst shows the evolution of nitrogen by NO decomposition as well as stored NO reacting with H_2 to form adsorbed N and eventually N_2. A large fraction of N_2 is produced via NH_3 as an intermediate.

The results clearly show the existence of concentration gradients and transport in the storage phase. The extent to which the stored NO_X transport limits the storage and/or reduction will depend on the conditions such as temperature, storage and reduction timing and catalyst properties such as Pt particle size distribution and loading. This speculative picture will be quantified in the work to be presented elsewhere.

Disclaimer

Acknowledgments

This study was jointly funded by BASF Catalysts LLC (formerly Engelhard Inc.) and the US DOE National Energy Technology Laboratory (DE-FC26-05NT42630) with partial support from the National Science Foundation (CT50730824). We would like to thank Stan Roth and CZ Wan from BASF Catalysts LLC for engaging technical interactions and for the catalytic materials used in this study.

References

[1] K.S. Kabin, P. Khanna, R.L. Muncrief, V. Medhekar, M.P. Harold, Catal. Today 114 (2006) 72.
[2] R.L. Muncrief, P. Khanna, K.S. Kabin, M.P. Harold, Catal. Today 98 (2004) 393.
[3] L. Olsson, H. Persson, E. Fridell, M. Skoglundh, B. Andersson, J. Phys. Chem. B 105 (2001) 6895.
[4] L. Olsson, E. Fridell, J. Catal. 210 (2002) 340.
[5] W.S. Epling, L.E. Campbell, A. Yezerets, N.W. Currier, J.E. Parks II, Catal. Rev. Sci. Eng. 46 (2) (2004) 163.
[6] A. Güthenke, D. Chatterjee, M. Weibel, B. Krutzsch, P. Kocí, M. Marek, I. Nova, E. Tronconi, B.M. Guy, Adv. Chem. Eng., AP 33 (2008) 103.
[7] S. Roy, A. Baiker, Chem. Rev. 109 (2009) 4054.
[8] H. Mahzoul, J.F. Brilhac, P. Gilot, Appl. Catal. B 20 (1999) 47.
[9] J.T. Gleaves, J.R. Ebner, T.C. Kuechler, Catal. Rev. Sci. Eng. 30 (1988) 49.
[10] J.T. Gleaves, G.S. Yablonskii, P. Phanawadee, Y. Schuurman, Appl. Catal. A 160 (1997) 55.

[11] J.T. Gleaves, G. Yablonsky, X. Zheng, R. Fushimi, P.L. Mills, J. Mol. Catal. A: Chem. 315 (2010) 108.
[12] J. Pérez-Ramírez, E.V. Kondratenko, Catal. Today 121 (2007) 160.
[13] V. Medhekar, V. Balakotaiah, M.P. Harold, Catal. Today 121 (2007) 226.
[14] A. Kumar, V. Medhekar, M.P. Harold, V. Balakotaiah, Appl. Catal. B 90 (2009) 642.
[15] J.P. Breen, R. Burch, C. Hardacre, C.J. Hill, C. Rioche, J. Catal. 246 (2007) 1.
[16] N.W. Cant, I.O.Y. Liu, M.J. Patterson, J. Catal. 243 (2006) 309.
[17] P. Forzatti, L. Castoldi, I. Nova, L. Lietti, E. Tronconi, Catal. Today 117 (2006) 316.
[18] A. Lindholm, N.W. Currier, J. Li, A. Yezerets, L. Olsson, J. Catal. 258 (2008) 273.
[19] D. Bhatia, R.D. Clayton, M.P. Harold, V. Balakotaiah, Catal. Today 147S (2009) S250.
[20] Y. Sakamoto, K. Okumura, Y. Kizaki, S. Matsunaga, N. Takahashi, H. Shinjoh, J. Catal. 238 (2006) 361.
[21] G. Zhou, T. Luo, R.J. Gorte, Appl. Catal. B 64 (2006) 88.
[22] I. Nova, L. Castoldi, L. Lietti, E. Tronconi, P. Forzatti, F. Prinetto, G. Ghiotti, J. Catal. 222 (2004) 377.
[23] L. Olsson, H. Persson, E. Fridell, M. Skoglundh, B. Andersson, J. Phys. Chem. B 105 (2001) 6895.
[24] R. Clayton, M.P. Harold, V. Balakotaiah, Appl. Catal. B 81 (2008) 161.
[25] W.P. Partridge, J.-S. Choi, Appl. Catal. B 91 (2009) 144.
[26] D. James, E. Fourre, M. Ishii, M. Bowker, Appl. Catal. B 45 (2003) 147.
[27] L. Cumaranatunge, S.S. Mulla, A. Yezerets, N.W. Currier, W.N. Delgass, F.H. Ribeiro, J. Catal. 246 (2007) 29.
[28] R.D. Clayton, M.P. Harold, V. Balakotaiah, Appl. Catal. B 84 (2008) 616.
[29] L. Lietti, I. Nova, P. Forzatti, J. Catal. 257 (2008) 270.
[30] R.D. Clayton, M.P. Harold, V. Balakotaiah, C.Z. Wan, Appl. Catal. B 90 (2009) 662.
[31] D. Bhatia, M.P. Harold, V. Balakotaiah, Catal. Today, accepted.